FLUTTER ASSESSMENT OF A ROTOR BLADE IN HOVER BASED ON INDICIAL AERODYNAMICS CONSIDERING BLADE PROFILE, ROTOR INFLOW AND WAKE PERIODICITY

Jürgen Arnold, Juergen.Arnold@dlr.de, DLR German Aerospace Center (Germany)

Abstract

The 7AD rotor blade is assessed for flutter stability in hover. For the aeroelastic analyses, the multibody model is tightly-coupled with an unsteady aerodynamic model based on Wagner's function and related enhancements for the general motion of an airfoil section considering heave and pitch. The mathematical setup of the Wagner function is extended for axial flow to include unsteady contributions related to rotor inflow and wake periodicity. Since the unsteady aerodynamic model is based on indicial functions, a separation of these contributions is possible and allows to study their individual impact on rotor blade flutter. According flutter results are extracted in frequency domain for three test cases which differ in the unsteady aerodynamic model for circulation comprising blade profile, rotor inflow and wake periodicity. As known for articulated rotor blades, also the 7AD blade exhibits a classical bending-torsion coupling. The lowest flutter onset is found for unsteady aerodynamics limited to blade profile, whilst the cases with added rotor inflow and wake periodicity show both the same flutter onset at a 5 % larger rotor speed. Here, the influence of rotor inflow plays the major role, since it increases the torsion damping within the critical flutter coupling. Added wake periodicity neither changes frequency nor damping and hence, does not affect the aeroelastic coupling.

1. INTRODUCTION

This paper summarizes the aeroelastic modelling and steps performed towards an improved flutter assessment of the 7AD rotor model in hover utilizing a multibody system (MBS). The objective is the stability assessment of the elastic rotor blade using tight coupling between the multibody system and an unsteady aerodynamic model based on indicial functions [1] for rotor blade sections. The aerodynamic model has been developed at the DLR Institute of Aeroelasticity and used for the stability analyses of isolated rotor setups with straight [2] and double-swept rotor blades [3] in the DLR projects FAST- and URBAN-Rescue before test entry. Here, the use of indicial functions allows to separate unsteady aerodynamic effects related to blade profile, rotor inflow as well as rotor wake periodicity and to study their influence on flutter onset.

The 7AD rotor was included in several European wind tunnel campaigns and operated in different setups as isolated or main rotor of a complete helicopter configuration. Also, the known GOAHEAD experimental setup [4] in the DNW-LLF wind tunnel from Figure 1 made intensive use of this articulated rotor. An earlier contribution [5] already dealt with the flutter assessment of the isolated 7AD rotor in hover and the available MBS model forms now the basis for the first application of the new unsteady aerodynamic model which is based on the extended Wagner function for axial rotor flow.

Figure 1: 7AD rotor in the GOAHEAD setup.

Presented at 47th European Rotorcraft Forum, United Kingdom, 7-9th September, 2021

In general, major improvement of the overall prediction capability for dynamic and aeroelastic simulation of rotorcraft is available by means of a multibody system for the setup of the mechanical model [6]-[7] which is characterized by connected rotary and non-rotary substructures. The application of multibody dynamics allows the consideration of all non-linear contributions relevant in a rotating system like geometric stiffening of the flexible blades and additional damping terms activated by gyroscopic effects as well as the provision of a correct mechanical interface between the rotating and non-rotating frames by applying non-linear joint definitions. Here, the multibody system SIMPACK [8]-[9] is used for the setup and simulation of the mechanical model of the 7AD rotor with its flexible blades. Flexibility of the non-rotating blade is described in the multibody system SIMPACK with a modal approach for available finite element models. For the assessment of the rotor in axial inflow condition, an unsteady theory using indicial aerodynamics based on the extended Wagner function in combination with steady two-dimensional airfoil data is applied to the multibody model. This approach allows an efficient and robust flutter assessment of DLR rotor setups in the design process and before entry into service, but is currently limited to hover.

2. NUMERICAL METHODS

2.1. Multibody Dynamics

The multibody system SIMPACK [8]-[9] is used to set up and simulate the mechanical model of the rotor with its flexible rotor blades including large rigid body motions of the rotor hub and blade hinges as well as small deformations of the elastic structure. The development of the simulation package was originally initiated by DLR and later out-sourced for further development and commercial distribution.

Flexibility of the non-rotating blade is described in the multibody system SIMPACK with a modal approach [10]-[11] for available finite element models. Several features allow the introduction of elastic rotor blades:

(A) Implementation of complete elastic blade as one elastic body and additional geometric stiffness terms via standard FlexModal interface

(B) Implementation of elastic blade with connected elastic substructures via standard FlexModal interface

(C) Application of the intrinsic elastic beam model SIMBEAM

(D) Application of the Rotor Blade Generator based on SIMBEAM

Feature (A) allows the straight-forward use of finite element models of industrial model size. Currently, the FlexModal interface supports ABAQUS, ANSYS, MSC.NASTRAN, NX.NASTRAN, PERMAS and RADIOSS. The feature (B) might be advantageous to add further non-linear characteristics of the multibody joints that interconnect elastic substructures. In addition, feature (C) and (D) provide a solution, if a finite element code is not available or is not supported by FlexModal. In the present work, SIMPACK 2021 has been used.

Feature (A) which is based on the implementation of the complete elastic model together with additional geometric stiffness using the FlexModal interface is chosen for the 7AD rotor blades. Two FEM solutions from a preprocessing step with the finite element code MSC.NASTRAN are required in order to process the blade:

- A modal solution provides the modal elastic model with natural frequencies and mode shapes for the non-rotating blade at Ω=0 Hz.
- A static solution provides the geometric stiffness terms for the description in the relevant degrees-of-freedom of the rotating blade for Ω>0 Hz (centrifugal forces due to angular velocity).

FlexModal reads the model geometry, mass and stiffness matrices, natural frequencies, mode shapes, geometric stiffening terms and the used load case entries for the derivation of the geometric stiffening terms from the pre-processed finite element data. Then, FlexModal translates this input into a common flexibility description which is based on the Standard Input Data (SID) format as described in [11]. The file containing the flexible substructure is added in SIMPACK with marker locations which are the same as found at the node positions in the finite element model, changing a rigid into an elastic body. Regarding aspects of component modal synthesis and substructuring, any hybrid model consisting of rigid and flexible bodies can be built. Rigid bodies can be made flexible by the introduction of a modal elastic model as described above or spring stiffness can be applied to a joint between two bodies from the MBS element library. SIMPACK adds the additional equations for the modal degrees-of-freedom to the set of differential algebraic equations (DAE) and solves the resulting set of equations.

2.2. Indicial Aerodynamics

An unsteady theory using indicial aerodynamics based on Wagner's function [1] in combination with steady two-dimensional airfoil data is applied to the multibody model. The fast aerodynamic model is based on radial independent strips and has been implemented using the approximation of R.T. Jones

for Wagner's function [2]-[3]. This function considers a two-dimensional thin airfoil in impulsive motion from rest to uniform velocity and is commonly used as a model to describe the unsteady lift development for a change in angle-of-attack with fixed wing problems. According to Y.C. Fung [12], the description of unsteady lift is extended from an impulsive to a general motion including both, pitch and heave motion by considering unsteady apparent mass terms. All indicial response functions represent the circulatory parts of unsteady lift, are implemented in terms of a state space formulation as User Force Element (UFEL) in MBS SIMPACK and extended for rotors under axial flow condition. Related contributions include blade profile from the Wagner function [13], axial dynamic inflow from a non-linear differential equation [1] derived out of the results gained by Carpenter and Fridovich [14], and wake periodicity as modelled in Loewy's function [15]. All circulatory contributions are considered as dynamic states in the MBS.

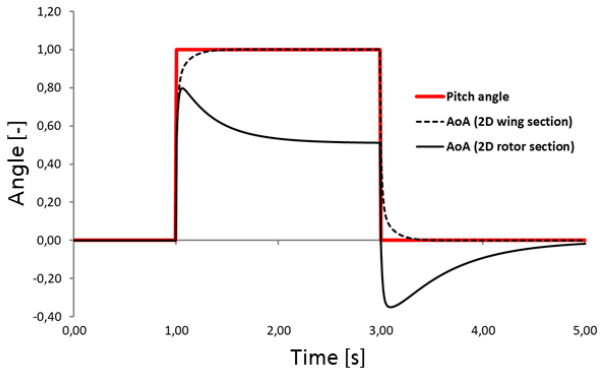

Figure 2: Temporal development of angle-of-attack (AoA) for pitch step input due to axial inflow dynamics.

The influence of added rotor inflow on the development of unsteady lift is obtained by applying pitch step excitations in the SIMPACK force element and evaluating the temporal development for the angle-of-attack which is a measure for lift and can be compared to the pitch input. Here, the indicial response for the Wagner function and axial dynamic inflow interacts depending on two separate scales for reduced time which is faster for the contribution from Wagner's function (rotor in-plane dynamics) and slower for axial inflow (rotor out-of-plane dynamics). As illustrated in Figure 2, dynamic axial inflow reduces the effective angle-of-attack for the rotor section, whilst a wing section without inflow follows the basic Wagner function and reaches the commanded pitch angle. Hence, the onset of rotor inflow decreases the angle-of-attack towards a steady value which represents the so-called lift deficiency [16] of a rotor under axial inflow. To complete the extension of Wagner's function to axial rotor flow, the periodicity term from Loewy's function [15] is implemented in the state space model of the SIMPACK force element. The finalized model was carefully tested for harmonic pitch oscillation to gain aerodynamic transfer functions for comparison of the basic Wagner function with the extended models. As an example, Figure 3 shows the lift amplitudes and phase angles versus rotor harmonics for a one-bladed rotor. The influence of inflow and periodicity can be clearly seen in both, lift amplitude and phase angle. Similar results with higher harmonic content are obtained for an increased number of blades.

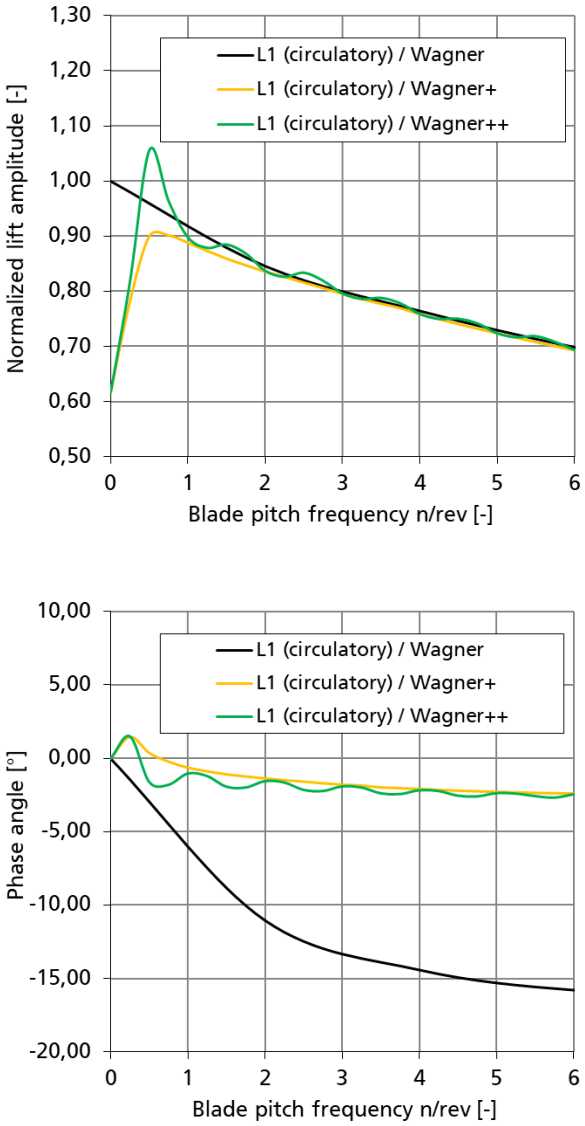

Figure 3: Unsteady lift amplitudes and phase angles of one-bladed rotor obtained with Wagner function and extensions for rotor inflow (+) and wake periodicity (++).

2.3. Aeroelastic Assessment

Standard features in MBS SIMPACK allow the aeroelastic assessment in a tightly-coupled manner on equation level of the rotor blades for axial inflow condition in both, frequency and time domain. The

approach in frequency domain which is based on linearization, consecutive analysis of the eigenbehaviour and stability rating from damping values can be followed here, since the system matrices for the symmetric rotor with axial inflow remain time invariant and the unsteady aerodynamic forces are considered in the dynamic state set. The analysis in frequency domain with the intrinsic eigensolver delivers typical flutter results in terms of frequency and damping plots. In general, these allow the verification of frequency placement and stability for the aeroelastic rotor system.

3. MODELS AND RESULTS

3.1. Dynamic and Aerodynamic Models

The mechanical setup of the 7AD rotor system is depicted in Figure 4 and consists of the flexible rotor blades and a rigid model for the DLR-ONERA rotor hub that is improved with measured values [17] for pitch link and lagging spring stiffness as well as lagging damping. The rotor hub is modelled with SIMPACK features to close the kinematic loop comprising of lead-lag hinge, flap hinge and pitch bearing via the pitch link to the swash plate. The flexibility of the non-rotating blade is described in the multibody system with a modal approach from a real modes solution and additional geometric stiffness contributions for the rotating blade are considered by static load cases for the relevant degrees of freedom, both computed in a pre-processing step with the finite element software MSC.NASTRAN. Further, the centrifugal pitching moment is considered at each radial marker via a SIMPACK Expression.

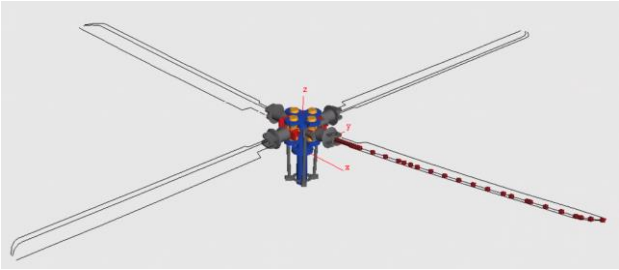

Figure 4: Multibody model of articulated 7AD rotor.

The four bladed rotor has a diameter of 4.2 m, mean blade chord of 0.14 m and a solidity of 0.085. Both blade hinges are located at a radius of 0.075 m and the blade attachment is found at the radial station of 0.275 m. The blade mass is approximately 3.18 kg. Figure 5 shows the MSC.NASTRAN beam model of the 7AD rotor blade along the straight blade axis and curved blade tip with additional rigidly connected nodes to model trailing and leading edge positions for spatial coupling.

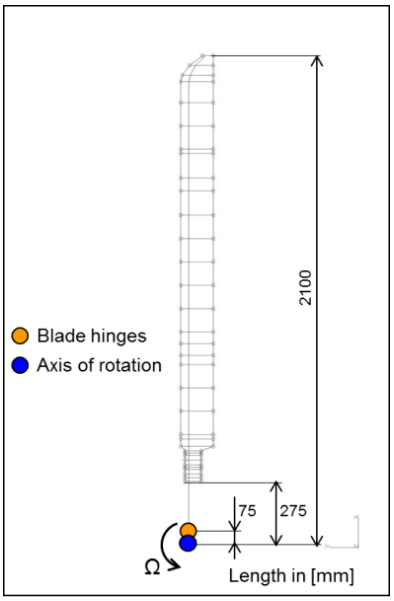

Figure 5: Finite element model with rigidly connected leading and trailing edge.

As described earlier by the author [5], measured vibration data is available from a ground vibration test (GVT) with rowing hammer technique for the clamped blade comprising modal properties in terms of natural frequencies and mode shapes for the non-rotating 7AD rotor blade. The comparison of simulation results for the clamped beam model with the experimental modal data takes the measured frequencies into account and global stiffness parameters of the finite element models are adjusted with respect to modulus of elasticity and shear, if necessary. The natural frequencies for the elastic blade modes obtained with the finite element and multibody model are given in Table 1 in terms of a relative frequency deviation with respect to the GVT results as reference values.

Mode	f_{GVT} [-]	f_{FEM} [-]	f_{MBS} [-]
1 / F1	1.000	0.980	0.980
2 / L1	1.000	1.009	1.009
3 / F2	1.000	1.015	1.015
4 / F3	1.000	0.991	0.991
5 / T1	1.000	0.996	0.996
6 / F4	1.000	1.034	1.034
7 / L2	1.000	1.062	1.062
8 / F5	1.000	1.004	1.004
9 / F6	1.000	0.995	0.995
10 / T2	1.000	0.959	0.959
(F = flap mode / L = lag mode / T = torsion mode)			

Table 1: Comparison of calculated frequencies with GVT data for clamped rotor blade.

Each rotor blade is equipped with 34 SIMPACK User Force Elements along the straight blade axis and the parabolic tip section. They provide the unsteady aerodynamic forces from circulation based on the extended Wagner function and related non-circulatory enhancements for the general motion of the airfoil section taking heave and pitch into account. The unsteady aerodynamic contributions based on circulation include blade profile, axial rotor inflow and wake periodicity from rotor blade interaction. Here, indicial functions allow to separate these effects into three cases according to Table 2 and to study their individual impact on rotor blade flutter.

Case	1 / Wagner	2 / Wagner+	3 / Wagner++
Blade profile	x	x	x
Rotor inflow		x	x
Wake periodicity			x

Table 2: Test cases for unsteady aerodynamic model.

3.2. Dynamic Simulation Results

The dynamic simulation results for hover are gained from the application of linearization features in MBS SIMPACK and show the development of the rotor frequencies versus nominal rotor speed for the dynamic rotor setup. As preparatory steps, an equilibrium computation for the derivation of the dynamic model states followed by a preload computation are performed to adjust the rotor model to the chosen rotor speed.

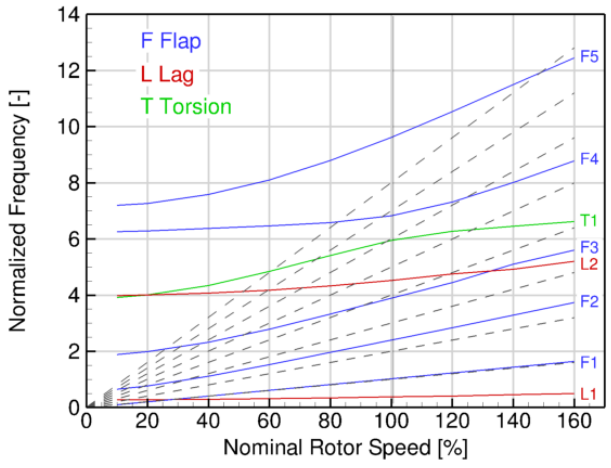

Figure 6: Rotor frequencies for the dynamic model from linearization.

The normalized frequencies of the 7AD rotor are found in Figure 6 and correlate well with other results [18] available inside DLR. Here, the plotted modes are numbered in ascending frequency order and the colour code describes the major motion contribution in terms of blade lag (red), flap (blue) and torsion (green) at nominal rotor speed. Hence, the mode assigned as first elastic torsion T1 represents the flap bending mode F4 for rotor speeds below the nominal operation speed, and vice versa. The dashed lines show the rotor harmonics up to 8/rev and allow the verification of the frequency placement for the 7AD dynamic rotor setup.

3.3. Aeroelastic Simulation Results

The aeroelastic simulation results for rotor hover are shown in Figure 7 to Figure 9 and comprise the development of the 7AD rotor frequencies and natural damping versus nominal rotor speed for the three studied aeroelastic setups. Again, they are processed using available SIMPACK linearization features together with two preceding simulation steps to derive an equilibrium for all dynamic states including indicial aerodynamics and then to preload the rotor with the appropriate aerodynamic and centrifugal loads for the chosen rotor speed. As listed in Table 2, the flutter diagrams are extracted for three test cases which differ in the unsteady aerodynamic model for circulation comprising the basic Wagner function and two extensions for axial rotor inflow and wake periodicity. Here, the unsteady motion parts from the SIMPACK User Force Element are considered by aerodynamic lag states which are found as real parts in the linearization result and thus, influence the blade damping. As mentioned before, the dynamic rotor setup includes a measured value for lagging damping which introduces the large damping found with both lead-lag modes L1 and L2. Similar to an earlier assessment of the 7AD rotor [5] utilizing Wagner's function and apparent mass contributions for unsteady aerodynamics, a pitch setting of around 3.70° at nominal rotor speed is chosen for the three cases. Due to the refined aerodynamic modelling which is especially found in the curved region of the blade tip, the new results show some differences. These comprise a first flap bending frequency F1 which is now slightly larger than 1/rev, inverted damping values for the lead-lag modes L1 and L2 as well as a coupling of L2 with the flap bending mode F3 for large rotor speeds.

The simulation results for Case 1 based on Wagner's function and non-circulatory apparent mass consider the unsteady aerodynamic contributions for the blade profile and are depicted in Figure 7. The flutter diagrams for the aeroelastic model comprise rotor frequencies and damping. In general, both curves allow the verification of frequency placement and stability for the aeroelastic rotor system. In comparison to the rotor frequencies from the dynamic simulation as presented in Figure 6, all bending modes show larger frequencies except for

mode F4. Here, the frequency slightly decreases at 100% of nominal rotor speed and indicates an aeroelastic coupling of bending mode F4 with torsion mode T1 for which the frequency increases. Above nominal rotor speed, the frequency of T1 is decreased what indicates now a coupling with bending mode F3 towards larger rotor speeds. In contrast, the frequency curves of both lead-lag modes remain unaltered. As already implied by the frequency behaviour of the aeroelastic model, the damping curves reveal a classical bending-torsion coupling of the third flap bending mode F3 and the first torsion mode T1 as known for articulated rotor blades. This mode pair becomes instable at 151 % rotor speed. The flutter coupling can be verified by switching off F3 and then, the negative damping of mode T1 disappears. Similar to the frequency curves of F4 and T1, the damping values for flap bending mode F4 represent those of torsion T1 below the nominal operation speed, and vice versa. In addition, a slight coupling is found between flap mode F3 and lead-lag mode L2 starting around the nominal rotor speed of 120 % which remains stable. Finally, the first flap mode F1 shows very large values of natural damping of around 30 % and hence, is not depicted in the plot.

The simulation results for Case 2 utilizing Wagner's function, rotor inflow and non-circulatory apparent mass consider unsteady aerodynamic contributions for blade profile and axial rotor inflow. According flutter diagrams are found in Figure 8 which are compared to the results of Case 1 that neglected the rotor inflow. Here, the rotor frequencies for the flap bending modes F2 and F4 show larger frequencies for Case 2, whilst the frequencies for F3, F5 and the torsion mode T1 decrease. As seen in the frequency increase of flap bending mode F4 and decrease of torsion mode T1 at 100% of nominal rotor speed, their aeroelastic coupling is less pronounced with axial inflow. Above the operation speed of 100 %, the frequency of T1 is decreased what indicates again the coupling with bending mode F3 towards larger rotor speeds. All other modes comprising F1, L1 and L2 remain more or less unchanged in their frequency behaviour. As before, the damping curves reveal the bending-torsion coupling of the third flap bending mode F3 and the first torsion mode T1 with flutter onset at 158 % of nominal rotor speed. As for the frequency curves of F4 and T1, also the damping values for flap bending mode F4 represent those of torsion T1 below the nominal operation speed, and vice versa.

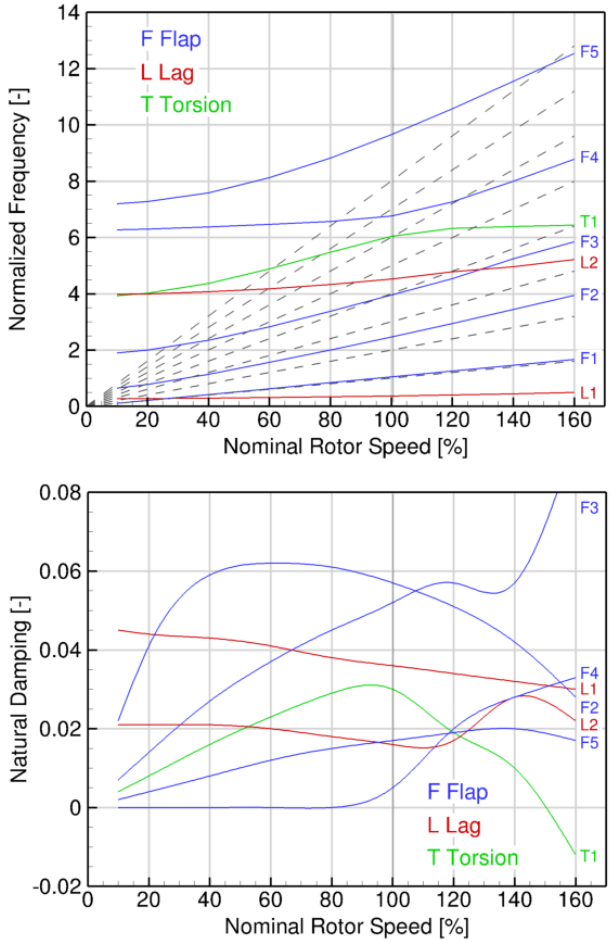

Figure 7: Rotor frequencies and damping for the aeroelastic model from linearization (Case 1 / Wagner).

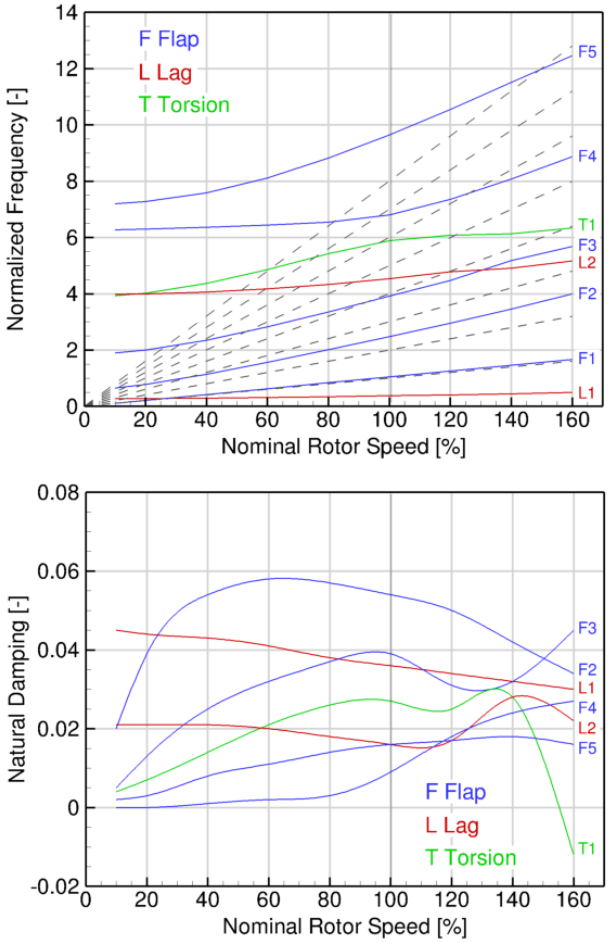

Figure 8: Rotor frequencies and damping for the aeroelastic model from linearization (Case 2 / Wagner+).

In general, the torsion mode T1 is higher damped for all rotor speeds and elastic flap bending modes (F2 - F5) are less damped than before, whilst damping remains rather the same for the rigid flap mode F1 as well as for both lead-lag modes L1 and L2. Again, a minor coupling of flap mode F3 and lead-lag mode L2 develops at the nominal rotor speed of 120 % which is stable within the studied speed range. Also, the flap mode F1 is not found in the plot, since it reaches large damping values around 30 %. To summarize the comparison to Case 1 in terms of rotor blade flutter in hover, it can be stated for the assessment of the 7AD rotor that the introduction of axial rotor inflow with Case 2 decreases the damping of the elastic flap bending modes, but increases torsion damping. As a result, the flutter onset is shifted to a larger rotor speed.

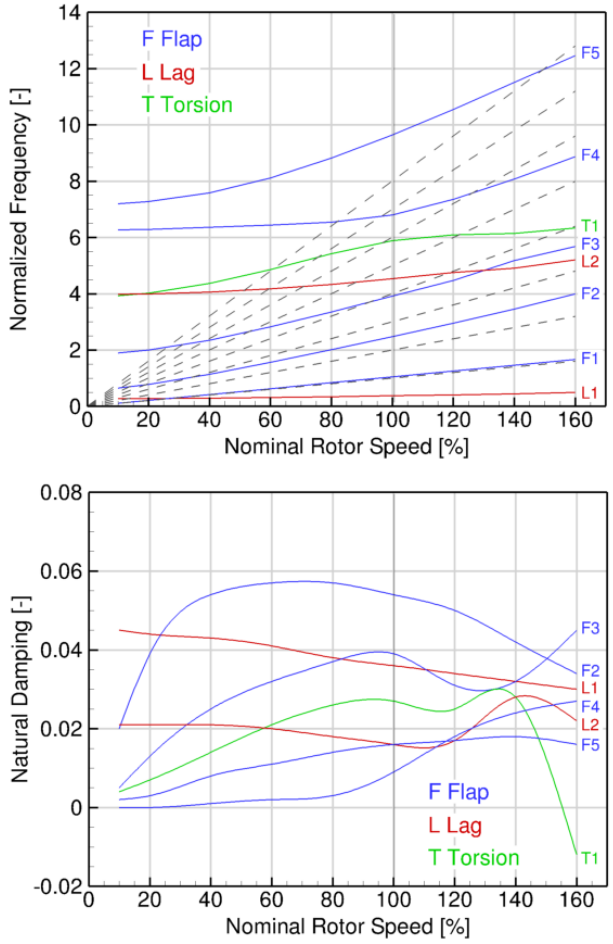

Figure 9: Rotor frequencies and damping for the aeroelastic model from linearization (Case 3 / Wagner++).

The simulation results for Case 3 using Wagner's function, rotor inflow, wake periodicity and non-circulatory apparent mass consider the unsteady aerodynamic contributions for blade profile, axial rotor inflow and wake periodicity. According flutter diagrams are found in Figure 9 which are compared to the results of Case 2 that do not take the influence of wake periodicity into account. The obtained frequency results are the same for all modes as found before with Case 2 except for the first torsion mode T1 which shows a very small increase between the nominal rotor speeds of 120 % and 140 %. Also, the computed damping results are the same as known from Case 2 except for a slight decrease for flap mode F2 at 60 % of nominal rotor speed. As before, the rigid flap mode F1 shows large natural damping values around 30 % and is not plotted. As a summary of the comparison to Case 2, it can be stated for the flutter assessment of the 7AD rotor in hover that the added wake periodicity within Case 3 does neither change the frequency nor the damping behaviour of the aeroelastic rotor system. Hence, the flutter onset at the nominal rotor speed of 158 % is the same as found for Case 2.

Finally, flutter onset gained for the three test cases of the 7AD rotor in hover is compared in Table 3. The lowest flutter onset is found for unsteady aerodynamics limited to the blade profile at a nominal rotor speed of 151 % (Case 1 / Wagner), whilst the two other cases with added rotor inflow and wake periodicity show both flutter at 158 % (Case 2 / Wagner+, Case 3 / Wagner++). Here, the influence of rotor inflow plays the major role, since it increases the torsion damping within the critical flutter coupling and shifts the flutter onset to an approximately 5 % larger rotor speed. For the studied 7AD rotor configuration in hover, added wake periodicity within Case 3 does neither change frequency nor damping and hence, does not affect the aeroelastic coupling in terms of a change in flutter speed.

Case	1 / Wagner	2 / Wagner+	3 / Wagner++
Blade profile	x	x	x
Rotor inflow		x	x
Wake periodicity			x
Flutter onset	151 %	158 %	158 %

Table 3: Flutter onset for unsteady aerodynamic models.

4. CONCLUSIONS AND OUTLOOK

The 7AD rotor blade has been assessed for flutter stability in hover. For the aeroelastic analyses, the multibody model was tightly-coupled with an unsteady aerodynamic model based on Wagner's function and related enhancements for the general motion of an airfoil section considering heave and pitch. Further, the used mathematical setup of the Wagner function in state space was extended for axial flow to include unsteady contributions related to rotor inflow and wake periodicity next to blade profile.

Since the unsteady aerodynamic model is based on indicial functions, a separation of these contributions is possible and allows to study their individual impact on rotor blade flutter. According flutter diagrams are extracted in frequency domain for three test cases which differ in the unsteady aerodynamic model for circulation comprising blade profile, rotor inflow and wake periodicity.

As well known for articulated blades, also the straight 7AD rotor blade with parabolic blade tip exhibits the classical bending-torsion coupling. The lowest flutter onset is found for unsteady aerodynamics limited to the blade profile at a nominal rotor speed of 151 % (Case 1 / Wagner), whilst the two other cases with added rotor inflow and wake periodicity show both flutter at 158 % (Case 2 / Wagner+, Case 3 / Wagner++). Here, the influence of rotor inflow plays the major role, since it increases the torsion damping within the critical flutter coupling and shifts the flutter onset to an approximately 5 % larger rotor speed. For the studied 7AD rotor configuration in hover, added wake periodicity neither changes frequency nor damping and hence, does not affect the aeroelastic coupling in terms of a change in flutter speed.

Future investigations related to the 7AD rotor blade comprise the influence of blade tip shape and wake periodicity on the resulting aeroelastic couplings. All damping plots show a coupling between lead-lag mode L2 and flap bending mode F3 which might be related to the local dynamics and aerodynamics of the parabolic blade tip. Hence, this coupling could disappear for the rectangular 7A layout which equals the 7AD blade except for the curved blade tip. Further, wake periodicity as modelled with the extended Wagner function does not influence the flutter speed in hover. This might change in forward flight where a broader harmonic content is activated.

5. REFERENCES

[1] Leishman JG. Principles of Helicopter Aerodynamics. Cambridge University Press, New York, 2nd edition, Chapter 8, 2000.

[2] Arnold J, Waitz S. Using Multibody Dynamics for the Stability Assessment of a New Rotor Test Rig. 43rd European Rotorcraft Forum, Milan, 2017.

[3] Arnold J, Waitz S. Using Multibody Dynamics for the Stability Assessment of a New Double-Swept Rotor Blade Setup. 44th European Rotorcraft Forum, Delft, 2018.

[4] Schwarz T, Pahlke K. CFD code validation for complete helicopters - The European GOAHEAD project. 67th American Helicopter Society Forum, Virginia Beach, Virginia, 2011.

[5] Arnold J. Flutter Assessment of a Rotor Blade with Innovative Layout in Hover using Indicial Aerodynamics. 72nd American Helicopter Society Forum, West Palm Beach, Florida, 2016.

[6] Morillo J, Singh R, Wasikowski M. Model Development and Integration of DYMORE at Bell Helicopter. 64th American Helicopter Society Forum, Montréal, 2008.

[7] Waitz S. The structural dynamics of a free flying helicopter in MBS- and FEM-analysis. 39th European Rotorcraft Forum, Moscow, 2013.

[8] Lugner P, Arnold M, Vaculin O (Eds). Vehicle System Dynamics (Special issue in memory Professor Willi Kortüm), Vol. 41, No. 5, 2004.

[9] https://www.3ds.com/products-services/simulia/products/simpack/

[10] Schwertassek R, Wallrapp O. Dynamik flexibler Mehrkörpersysteme. Vieweg, 1999.

[11] Wallrapp O. Standardization of Flexible Body Modeling in Multibody System Codes, Part I: Definition of Standard Input Data, Mechanics of Structures and Machines, 22(3), pp. 283-304, 1994.

[12] Fung YC. An Introduction to the Theory of Aeroelasticity. Dover Publications Inc, New York, 1993, Chapter 6.

[13] Wagner H. Über die Entstehung des dynamischen Auftriebes von Tragflügeln, Zeitschrift für angewandte Mathematik und Mechanik, Band 5, Heft 1, 1925.

[14] Carpenter PJ, Fridovich B. Effect of a Rapid Blade Pitch Increase on the Thrust and Induced Velocity Response of a Full-Scale Helicopter Rotor. NACA TN 3044, 1953.

[15] Loewy RG. A Two-Dimensional Approximation to the Unsteady Aerodynamics of Rotary Wings. Journal of the Aeronautical Sciences, Vol. 24, No. 2, pp. 81-92, 1957.

[16] Miller RH. Rotor Blade Harmonic Air Loading. AIAA Journal, Vol. 2, No. 7, 1964.

[17] Hoffmann F, Opitz S. Documentation for AT4 Structural Properties. Version 1.1, DLR Institute of Flight Systems, 2010.

[18] Surrey S, Wendisch JH, Wienke F. Coupled fluid-structure simulations of a trimmed helicopter rotor in forward flight. Proc 19th DGLR symposium STAB, Munich, 2014.